HHS Public Access

Author manuscript

Ann Surg Oncol. Author manuscript; available in PMC 2018 July 01.

Published in final edited form as:

Ann Surg Oncol. 2018 July ; 25(7): 1880–1888. doi:10.1245/s10434-018-6453-2.

Intraoperative Pancreatic Cancer Detection using Tumor-Specific Multimodality Molecular Imaging

Willemieke S. Tummers, MD[1,2], **Sarah E. Miller, BS**[3], **Nutte T. Teraphongphom, Ph.D**[3], **Adam Gomez, MD**[4], **Idan Steinberg, Ph.D**[1], **David M. Huland, Ph.D**[1], **Steve Hong, MD**[3], **Sri-Rajasekhar Kothapalli, Ph.D**[1], **Alifia Hasan, MBA**[3], **Robert Ertsey, M.Sc**[3], **Bert A. Bonsing, MD, PhD**[2], **Alexander L. Vahrmeijer, MD, PhD**[2], **Rutger-Jan Swijnenburg, MD, PhD**[2], **Teri A. Longacre, MD**[4], **George A. Fisher, MD**[5], **Sanjiv S. Gambhir, MD, PhD**[6], **George A. Poultsides, MD**[7], and **Eben L. Rosenthal, MD, FACS**[3,8]

[1]Department of Radiology, Molecular Imaging Program at Stanford (MIPS), Stanford University, Stanford, CA [2]Department of Surgery, Leiden University Medical Center, Leiden, The Netherlands [3]Department of Otolaryngology, Stanford University, Stanford, CA [4]Department of Pathology, Stanford University, Stanford, CA [5]Department of Medical Oncology, Stanford University, Stanford, CA [6]Departments of Radiology, Bioengineering, and Materials Science & Engineering, Molecular Imaging Program at Stanford; Canary Center at Stanford for Early Cancer Detection, Stanford University, Stanford, CA [7]Department of Surgery, Stanford University, Stanford, CA [8]Stanford Cancer Center, Stanford University, Stanford, CA

Abstract

Background—Operative management of pancreatic ductal adenocarcinoma (PDAC) is complicated by several key decisions during the procedure. Identification of metastatic disease at the outset and, when none is found, complete (R0) resection of primary tumor are key to optimizing clinical outcomes. The use of tumor-targeted molecular imaging, based on photoacoustic and fluorescence optical imaging, can provide crucial information to the surgeon. The first-in-human use of multimodality molecular imaging for intraoperative detection of pancreatic cancer is reported using cetuximab-IRDye800, a near-infrared fluorescent agent that binds to epidermal growth factor receptor.

Methods—A dose-escalation study was performed to assess safety and feasibility of targeting and identifying PDAC in a tumor-specific manner using cetuximab-IRDye800 in patients undergoing surgical resection for pancreatic cancer. Patients received a loading dose of 100 mg of unlabeled cetuximab before infusion of cetuximab-IRDye800 (50 mg or 100 mg). Multi-instrument fluorescence imaging was performed throughout the surgery in addition to fluorescence and photoacoustic imaging ex vivo.

Electronic supplementary material The online version of this article (https://doi.org/10.1245/s10434-018-6453-2) contains supplementary material, which is available to authorized users.

AUTHOR CONTRIBUTIONS ELR, GAP, SSG, BAB, ALV, RJS and WST designed the research; WST, SEM, NT, AG, IS, DMH, SH, SRK, AH, RE, TAL, GAF, and GAP performed the research; and WST, SEM, and ELR analyzed data and wrote the paper.

DISCLOSURE The authors declare no potential conflicts of interest.

Results—Seven patients with resectable pancreatic masses suspected to be PDAC were enrolled in this study. Fluorescence imaging successfully identified tumor with a significantly higher mean fluorescence intensity in the tumor (0.09 ± 0.06) versus surrounding normal pancreatic tissue (0.02 ± 0.01), and pancreatitis (0.04 ± 0.01; $p < 0.001$), with a sensitivity of 96.1% and specificity of 67.0%. The mean photoacoustic signal in the tumor site was 3.7-fold higher than surrounding tissue.

Conclusions—The safety and feasibilty of intraoperative, tumor-specific detection of PDAC using cetuximab-IRDye800 with multimodal molecular imaging of the primary tumor and metastases was demonstrated.

Pancreatic ductal adenocarcinoma (PDAC) remains a highly lethal malignancy, with an expected median survival of 25 months for patients undergoing surgery with adjuvant chemotherapy.[1,2] After diagnosis of PDAC, patient selection for surgical resection is challenging at multiple stages during the procedure: detection of occult distant metastases, assessment of the extent of the primary tumor, peritumoral lymph nodes (LN), and the resection margins. Surgeons address two critical decisions during the procedure that will determine the long-term survival of pancreatic cancer: the absence of metastatic and regional disease and cancer-free margins.[3–5] However, margin-positive resections are a frequent phenomenon (which occurs up to 70% of cases),[6] as is the emergence of distant metastases soon after surgery.[7] Failure to identify small tumor extensions during surgery is not surprising, due to the growth pattern of the tumor and the inability of the surgeon to differentiate between tumor and (peritumoral) inflammation.

The use of tumor-targeted imaging probes for photoacoustic and optical imaging modalities has the potential to provide real-time information to the surgeon to aid decision making. Photoacoustic imaging can provide intraoperative or transcutaneous images with functional information at clinically relevant depths (up to 5 cm) with submillimeter spatial resolution.[8] Fluorescent optical imaging, on the other hand, is superior for imaging of superficial lesions with a very high resolution.[9]

Despite significant investment in systemic therapy for small incremental gains in survival, there has been minimal investment in improving surgical outcomes. Although the value of intraoperative guidance in pancreatic cancer resection would seem obvious, previous studies have not demonstrated benefit when using the nonspecific imaging agent indocyanine green (ICG).[10] Rosenthal et al. showed the successful use of cetuximab-IRDye800 to image sub-clinical fragments of squamous cell carcinoma arising in the head and neck cancer patients.[11] EGFR also is highly expressed in PDAC and is a good target for fluorescence imaging, due to its transmembrane position.[12–15] This study is the first example of tumor-specific multimodality molecular imaging for the accurate detection of primary PDAC, tumor-bearing LN, and distant metastases. The workflow of infusion, surgery, and imaging is shown in Fig. 1.

MATERIALS AND METHODS

Experimental Design

This study is a single-arm, open-label, dose-escalation study; the main objectives were to determine the safety and feasibility of tumor-specific multimodal molecular imaging for intraoperative detection of PDAC. Patients with suspected or biopsy-proven PDAC scheduled to undergo surgical resection at Stanford University Hospital were identified. A pretreatment dose of 100 mg of unlabeled cetuximab was administered before the study drug to differentiate between a cetuximab reaction and a cetuximab-IRDye800 reaction and to saturate the EGFR receptors in normal tissues with high expression (antigen sinks).[16] Two to five days after cetuximab-IRDye800 infusion, patients underwent surgery.

Investigational Agent: Cetuximab-IRDye800

The cetuximab-IRDye800 was produced under cGMP conditions at the University of Alabama (UAB) Vector Production Facility as previously described, before shipment to Stanford University Hospital Pharmacy (see also Supplementary Methods).[17]

Imaging

Intraoperative Near-Infrared (NIR) Imaging—Imaging during surgery was performed using the laparoscopic optical imaging system PINPOINT 9000 modified for IRDye800 fluorescent dye imaging (Novadaq, Burnaby, Canada), and the wide-field SurgVision Explorer (SurgVision BV, ‘t Harde, The Netherlands). During surgery, imaging was performed during inspection of the abdomen, before resection for the primary tumor, and after resection for the wound bed. This procedure is described in detail in the Supplementary Materials. Subsequently, all excised tissues were imaged ex vivo at a separate table in the OR directly after removal. Next, the surgical specimen was processed by the pathologist according to standard clinical practice to determine tumor status.

Ex vivo Close-field NIR Imaging—The Pearl Impulse imaging platform (LI–COR Biosciences, Lincoln, NE) was used to image fresh tissues obtained in the operating room before paraffin embedding. The procedure is described in the supplementary methods.

Ex Vivo Photoacoustic Imaging—After excision of the specimen, ex vivo photoacoustic imaging was performed on the primary specimen and breadloaf sections of the tumor using a Stanford-build clinical hand-held photoacoustic imaging (PAI) and ultrasound transducer as previously described.[18] For detailed description of the imaging analysis for both fluorescent and photoacoustic imaging, see Supplementary Methods.

Ethics Approval

This study is performed in accordance with the tenets established by the Helsinki Declaration of 1975, ICH-GCP guidelines, and the laws and regulations of the United States. The Stanford University Institutional Review Board and the FDA approved the study protocol. All patients provided written, informed consent before the start of any study-related procedures. The study was registered in the Clinical Trials Database of the U.S. National Institutes of Health, under number NCT02736578.

Pathologic Assessment

All resected lesions were examined for tumor status by a gastrointestinal pathologist with expertise in pancreatobiliary disease. A positive tumor that was fluorescent was considered a true positive, a negative lesion that was fluorescent was considered a false positive, and a positive tumor that was nonfluorescent was considered a false negative. Fluorescence positivity was determined based on the MFI of the raw data.

Histologic Correlation—Formalin-fixed, paraffin-embedded tumor tissues were sectioned at 4-μm thickness and fluorescence imaging was performed using the Odyssey NIR scanner (Li-COR Biosciences). All histologic sections were stained with standard hematoxylin–eosin (H&E). To confirm the presence of EGFR, additional sections underwent immunohistochemical (IHC) analysis for EGFR expression utilizing anti-human EGFR. In addition, Ki-67 proliferation index was determined by IHC. See Supplementary Methods for further details. Appropriate positive and negative controls were included and evaluated with the specimens tested.

Fluorescence Microscopy—FFPE slides were prepared for fluorescence microscopy using the methods described in Supplementary Materials.

Adverse Events

Adverse events were classified according to the National Cancer Institute Common Terminology Criteria (Version 4.0), see Supplementary Methods.

Statistical Analysis

SPSS statistical software package (version 23.0, IBM Corp.) was used for statistical analyses. Differences in fluorescent signal per tissue type (tumor, pancreatitis, normal pancreatic tissue) were tested separately and between different dose groups, with one-way ANOVA with posthoc Bonferroni correction.

RESULTS

Patient and Safety Data

Between July 2016 and April 2017, ten patients were screened for trial eligibility. Eight patients with suspected PDAC received a loading dose Cetuximab, and seven were enrolled. One patient was not enrolled, because he had an infusion reaction on the loading dose Cetuximab. The other seven patients received cetuximab-IRDye800. Patient and tumor characteristics are summarized in Table 1; 5 received 50 mg of cetuximab-IRDye800 (cohort 1) and 2 received 100 mg of cetuximab-IRDye800. There was one CTCAE grade-2 adverse event in cohort 1: fever, possibly related to cetuximab or cetuximab-IRDye800. No other possibly related adverse events occurred (Table 1). Two patients had neuroendocrine tumors at pathologic assessment, and one patient did not undergo resection due to liver metastases. Consistent with the literature regarding cetuximab administration for therapeutic purposes, a small increase of QTc interval was seen after infusion of the loading dose cetuximab with no further increase after cetuximab-IRDye800.[19,20] QTc interval gradually decreased to baseline and none of the patients had persistent increased QTc after the observation period.

Intraoperative NIR Fluorescent Imaging

Laparoscopic NIR-imaging was performed at the diagnostic laparoscopy before resection. All surgeries, except one, were converted to an open procedure, and widefield NIR imaging was performed during the subsequent procedure. The primary pancreatic tumor and/or LN could be clearly identified in every patient: bright-field (Figs. 2a, e), overlay (Figs. 2b, f), grayscale (Figs. 2c, g), and heat-map (Fig. 2d, h). Fluorescence imaging provided a clear contrast between tumor and surrounding tissues for both the primary tumor and LN dissection. The primary tumor could be identified in four of the six patients during surgical resection, with mean TBR of 2.3 ± 0.72. In the other two patients, the tumor was situated below the peripancreatic fat (> 5-mm depth) and therefore was intraoperatively not visible using NIR fluorescence. During surgery, tumor-bearing LN could be identified with mean TBR of 6.3 ± 0.82. Back table imaging of the primary tumor in all patients demonstrated a mean TBR of 3.4 ± 0.4.

Correlation of Fluorescence with Histological Disease

Correlation between fluorescent signal and histologic evidence of disease was established using close-field fluorescence imaging (Fig. 3). The average fluorescent signal was significantly different in normal pancreatic tissue (MFI 0.02 ± 0.01), pancreatitis (MFI 0.04 ± 0.02), and tumor (MFI 0.09 ± 0.06) ($p < 0.001$) (Fig. 3K). This allows tumor detection with a sensitivity of 96.1% (CI 92.19–98.43%) and specificity of 67.0% (CI 59.69–73.81%). There was no significant difference in MFI between normal pancreatic tissue (MFI 0.02 ± 0.01; 0.03 ± 0.02), pancreatitis (MFI 0.03 ± 0.02; 0.06 ± 0.03), and PDAC (MFI 0.09 ± 0.06; 0.1 ± 0.05) between the low and high dose cohort, respectively. Tumor-bearing LN ($n = 29$) could be detected with significantly higher MFI (0.06 ± 0.01) compared with tumor-negative ($n = 78$) LN (0.02 ± 0.002) ($p < 0.001$; Fig. 3l). Interestingly, liver metastases could be detected as well by negative contrast (Fig. S1).

Ex vivo Photoacoustic Imaging

Ex vivo photoacoustic imaging of primary tumor and LN was performed using a custom built photoacoustic imaging system to determine the potential utility of this strategy for eventual in vivo use.[21] In this study, photoacoustic imaging could successfully be performed in all patients ($n = 4$). (The device was not available for two patients). There was a clear increase in photoacoustic imaging signal in the primary tumor compared with surrounding pancreatic tissue (Fig. S2) and in the tumor-bearing LN (Fig. 4), which was consistent with the optical fluorescence imaging results. The mean photoacoustic signal in the tumor (32,286 ± 1660 AU) was significantly higher compared to background (8651 ± 902 AU) ($p < 0.001$), which indicates a mean 3.7-fold increase in signal in the tumor compared to surrounding tissue (Fig. 4g). A difference in signal-to-noise ratio (SNR) was observed between patients, as shown in Fig. 4h. This trend was comparable to the difference in fluorescence imaging results in the same patients (Fig. S2 and S3D).

Molecular Correlation

The correlation of fluorescence on microscopic level (Fig. S3, panel I) was performed to correlate the uptake of the antibody-dye bioconjugate in the tumor but not surrounding

stromal elements. To perform this analysis, a grid was overlaid on the fluorescently scanned slides to determine the MFI per specific area and then mapped to the histological grid as shown in (Fig. S3, panel II). The tumor could be identified with a sensitivity of 95% (CI 92.8–96.8%), specificity of 61% (CI 58.8–63.2%), AUC of 0.84 (CI 0.82–0.85), and a positive- and negative-predicting values of 37.8 and 98.0%, respectively. MFI also was correlated with EGFR expression (Fig. S3, panel III). In Fig. S3D, the MFI per patient per tissue type is shown. A clear difference can be detected in MFI per patient. This is likely due to the heterogeneity of EGFR expression between tumors. Patient 4 had relatively strong EGFR expression, patients 5 and 6 had moderate EGFR expression, and patients 1–3 had low expression (Fig. S3E). Although low EGFR expression in the tumor is seen in those patients, a clear difference in the MFI between tumor and surrounding pancreatic tissue could be detected (Fig. S3D).

To localize cetuximab-IRDye800 within the tumor cells, we used fluorescence microscopy. Figure S4 shows representative images of the 800-nm fluorescent signal at the tumor ducts but not adjacent stromal tissues. Importantly, fluorescent signal (serving as a surrogate for the antibody-dye bioconjugate) is identified within the tumor ducts, indicating the successful antibody penetration into the tumor.

DISCUSSION

We demonstrated for the first time the safety and efficacy of tumor-specific multimodality molecular imaging in the detection of pancreatic cancer using NIR fluorescently-labeled antibody. Current metabolic and anatomic imaging modalities often fail to detect small tumor lesions or tumor-bearing LN, and as a result, intraoperative identification of the disease is critical to help guide decision making and precision surgery.

We found a significant difference in fluorescent signal between tumor-bearing and negative LN at the lower dose (50 mg); however, at the higher dose (100 mg), we observed an increased number of false-positive fluorescent LN. We hypothesize that this is caused by lymphatic drainage of excess antibody to the primary nodal basin, which is similar to findings with cetuximab-IRDye800 in head and neck cancer.[22] We have shown that this technique can guide tumor-bearing LN detection and removal when used at the optimal dose, which can be beneficial in patients with tumor-bearing LN in the first-echelon (N1).[23] Therefore, the optimal dose Cetuximab-IRDye800 established in this study is 50 mg, with a loading dose of 100 mg cetuximab. Due to variety of the infusion window in this study between cetuximab-IRDye800 infusion and surgery, no conclusion can be drawn if a specific timing is optimal. We can conclude that all intervals in the infusion window, 2–5 days before surgery, provide clear tumor-to-background ratios and therefore are sufficient for this purpose.

We have previously shown that EGFR has high levels of expression in the primary tumor and tumor-bearing LN, a finding that is confirmed by the results of our current study using EGFR as a target.[15] A difference in EGFR expression between neuroendocrine tumors and PDAC was seen (Fig. S3D) with lower expression in neuroendocrine tumors, resulting in subsequent lower absolute fluorescence signal. Nevertheless, in both patients with

neuroendocrine tumors, the background signal in normal pancreatic tissue was three times lower to provide sufficient TBRs for detection. High expression of EGFR in the stomach and duodenum resulted in high levels of background fluorescence in these organs. We hypothesize that this is located in normal luminal epithelium, because fluorescence correlated with EGFR and Ki-67 expression at this position (Fig. S5). Background fluorescence from these organs, however, did not interfere with detection of the primary tumor or LN during surgery, partly because the stomach and duodenum can be retracted away from the pancreatic tumor.

Furthermore, the potential of this technique to differentiate between PDAC and pancreatitis is crucial, because this is a difficult distinction to make both before surgery and intraoperatively, leading to approximately 7% of pancreatic resections being performed for benign conditions.[24] Fluorescence imaging also may add value for margin assessment: in one patient, a positive pancreatic neck margin was evident during back-table imaging with clear fluorescence being visualized in the pancreatic neck, also confirmed by ex vivo imaging at pathology (Fig. S6). This preliminary observation supports the notion that this technology may be useful for real-time identification of close or positive margins during resection, but future prospective studies are needed in this direction.

The observed negative contrast of tumor in the liver may be related to the intensity of fluorescence in the normal surrounding liver, because it is known that the amount of fluorescent dye coupled to EGFR targeting antibodies will influence the biodistribution of the conjugate. Our conjugate has a dye/protein ratio of 1.8, which indicates that some molecules will have two or more eq of dye coupled to the antibody.[17] Those are known to have the tendency for increased liver uptake.[25] Another explanation can be the difference in EGFR expression in the metastases, which was clearly lower than surrounding hepatocytes.

It is worth noting that cetuximab-IRDye800 clearly penetrates the tumor and reaches the tumor cells. Limited success rates of phase II-III clinical trials on PDAC are commonly attributed to the presence of dense desmoplastic stroma, consisting of cellular and acellular components.[26–31] This is thought to reduce severely the delivery of systemically administered therapies to the tumor and contribute the unresponsiveness of PDAC to systemic chemotherapy. We show at least to some extent that the EGFR monoclonal antibody can indeed reach the tumor successfully.

The main limitation of the study was the small sample size; however, it was sufficient for a proof-of-principle study investigating the safety and feasibility of multimodal molecular imaging in pancreatic cancer patients and to identify significant results in the detection of tumor, and tumor-bearing LN. A second limitation is based on the limited depth penetration of NIR fluorescent imaging. For pancreatic cancer, an imaging depth of 1 cm, achieved by fluorescence when used as single modality, is not enough to capture successfully the spatial features of the tumor. The combination with photoacoustic imaging can overcome the limited depth penetration.

CONCLUSIONS

This is the first-in-human study to evaluate the use of multimodality molecular imaging in patients undergoing surgical resection for pancreatic cancer. Our findings emphasize that the technique is safe and feasible for this pilot patient population. This type of tumor-specific imaging could be leveraged for a range of diagnostic techniques, including detection of metastatic disease, identification of the primary tumor and tumor-bearing LN, assessment of resection margins, and identification of residual disease at the tumor bed after resection. Whether this additional information can change surgical management over commonly used, conventional methods remains to be determined in future, prospective trials.

Supplementary Material

Refer to Web version on PubMed Central for supplementary material.

Acknowledgments

The authors acknowledge support from Stanford Cancer Institute Translational Research Grant, and Intuitive Surgical Clinical Robotics Research Grant. Tummers WS contribution to this work was supported in part by Michaël-van Vloten Fonds, Lisa Waller Hayes Foundation, Jo Kolk Studiefonds, McKinsey Grant, and Ketel1 Studiefonds. Huland DM contribution to this work was supported in part by NCI training grant: T32 CA118681.

References

1. Christians KK, et al. Survival of patients with resectable pancreatic cancer who received neoadjuvant therapy. Surgery. 2016; 159(3):893–900. [PubMed: 26602840]
2. Roeder F. Neoadjuvant radiotherapeutic strategies in pancreatic cancer. World J Gastrointest Oncol. 2016; 8(2):186–97. [PubMed: 26909133]
3. Bassi C, et al. Value of regional lymphadenectomy in pancreatic cancer. HPB (Oxford). 2005; 7(2): 87–92. [PubMed: 18333169]
4. Bachmann J, et al. Pancreatic resection for pancreatic cancer. HPB (Oxford). 2006; 8(5):346–51. [PubMed: 18333087]
5. Tummala P, Howard T, Agarwal B. Dramatic survival benefit related to R0 resection of pancreatic adenocarcinoma in patients with tumor B 25 mm in size and B 1 involved lymph nodes. Clin Transl Gastroenterol. 2013; 4:e33.
6. Verbeke CS, Gladhaug IP. Resection margin involvement and tumour origin in pancreatic head cancer. Br J Surg. 2012; 99(8):1036–49. [PubMed: 22517199]
7. Zhang JF, et al. Influence of perineural invasion on survival and recurrence in patients with resected pancreatic cancer. Asian Pac J Cancer Prev. 2013; 14(9):5133–9. [PubMed: 24175789]
8. Zackrisson S, van de Ven SM, Gambhir SS. Light in and sound out: emerging translational strategies for photoacoustic imaging. Cancer Res. 2014; 74(4):979–1004. [PubMed: 24514041]
9. Vahrmeijer AL, et al. Image-guided cancer surgery using near-infrared fluorescence. Nat Rev Clin Oncol. 2013; 10(9):507–18. [PubMed: 23881033]
10. Hutteman M, et al. Clinical translation of ex vivo sentinel lymph node mapping for colorectal cancer using invisible near-infrared fluorescence light. Ann Surg Oncol. 2011; 18(4):1006–14. [PubMed: 21080086]
11. Rosenthal EL, et al. Safety and tumor-specificity of cetuximab-IRDye800 for surgical navigation in head and neck cancer. Clin Cancer Res. 2015; 21(16):3658–66. [PubMed: 25904751]
12. Bloomston M, et al. Epidermal growth factor receptor expression in pancreatic carcinoma using tissue microarray technique. Dig Surg. 2006; 23(1–2):74–9. [PubMed: 16717472]
13. Uegaki K, et al. Clinicopathological significance of epidermal growth factor and its receptor in human pancreatic cancer. Anticancer Res. 1997; 17(5B):3841–7. [PubMed: 9427790]

14. de Geus SW, et al. Selecting tumor-specific molecular targets in pancreatic adenocarcinoma: paving the way for image-guided pancreatic surgery. Mol Imaging Biol. 2016; 18(6):807–19. [PubMed: 27130234]
15. Tummers WS, Boonstra MC, Prevoo HA, et al. Selection of optimal molecular targets for tumor-specific imaging in pancreatic ductal adenocarcinoma. Oncotarget. 2017; 8(34):56816–28. [PubMed: 28915633]
16. Moore LS, et al. Effects of an unlabeled loading dose on tumor-specific uptake of a fluorescently labeled antibody for optical surgical navigation. Mol Imaging Biol. 2016; 19(4):610–16.
17. Zinn KR, et al. IND-directed safety and biodistribution study of intravenously injected cetuximab-IRDye800 in cynomolgus macaques. Mol Imaging Biol. 2015; 17(1):49–57. [PubMed: 25080323]
18. Kothapalli SR, et al. Deep tissue photoacoustic imaging using a miniaturized 2-D capacitive micromachined ultrasonic transducer array. IEEE Trans Biomed Eng. 2012; 59(5):1199–204. [PubMed: 22249594]
19. Deeken JF, et al. Evaluation of the relationship between cetuximab therapy and corrected QT interval changes in patients with advanced malignancies from solid tumors. Cancer Chemother Pharmacol. 2013; 71(6):1473–83. [PubMed: 23589315]
20. Administration, U.S.F.a.D. ERBITUX$^{\grave{O}}$ (cetuximab) injection, for intravenous infusion—label. 2004. 2012 [cited 2017 July 27].
21. Kothapalli SR. Human prostate imaging using a novel integrated transrectal ultrasound and photoacoustic instrument. Nature Commun. 2017
22. Rosenthal E, et al. Sensitivity and specificity of Cetuximab-IRDye800CW to identify regional metastatic disease in head and neck cancer. Clin Cancer Res. 2017; 23(16):4744–52. [PubMed: 28446503]
23. Buchler P, Müller M, AlKhatib J, Buchler MW. Survival benefit of extended resection in pancreatic cancer. Am J Surg. 2007; 194:S120–6.
24. Gerritsen A, et al. Preoperative characteristics of patients with presumed pancreatic cancer but ultimately benign disease: a multicenter series of 344 pancreatoduodenectomies. Ann Surg Oncol. 2014; 21(12):3999–4006. [PubMed: 24871781]
25. Cohen R, et al. Inert coupling of IRDye800CW to monoclonal antibodies for clinical optical imaging of tumor targets. EJNMMI Res. 2011; 1(1):31. [PubMed: 22214225]
26. Philip PA. Targeted therapies for pancreatic cancer. Gastrointest Cancer Res. 2008; 2(4 Suppl):S16–9. [PubMed: 19343141]
27. Heinemann V, et al. Meta-analysis of randomized trials: evaluation of benefit from gemcitabine-based combination chemotherapy applied in advanced pancreatic cancer. BMC Cancer. 2008; 8:82. [PubMed: 18373843]
28. Von Hoff DD, et al. Increased survival in pancreatic cancer with nabpaclitaxel plus gemcitabine. N Engl J Med. 2013; 369(18):1691–703. [PubMed: 24131140]
29. Moore MJ, et al. Erlotinib plus gemcitabine compared with gemcitabine alone in patients with advanced pancreatic cancer: a phase III trial of the National Cancer Institute of Canada Clinical Trials Group. J Clin Oncol. 2007; 25(15):1960–6. [PubMed: 17452677]
30. Mitry E, et al. Safety and activity of masitinib in combination with gemcitabine in patients with advanced pancreatic cancer. Cancer Chemother Pharmacol. 2010; 66(2):395–403. [PubMed: 20364428]
31. Adiseshaiah PP, et al. Nanomedicine strategies to overcome the pathophysiological barriers of pancreatic cancer. Nat Rev Clin Oncol. 2016; 13(12):750–65. [PubMed: 27531700]

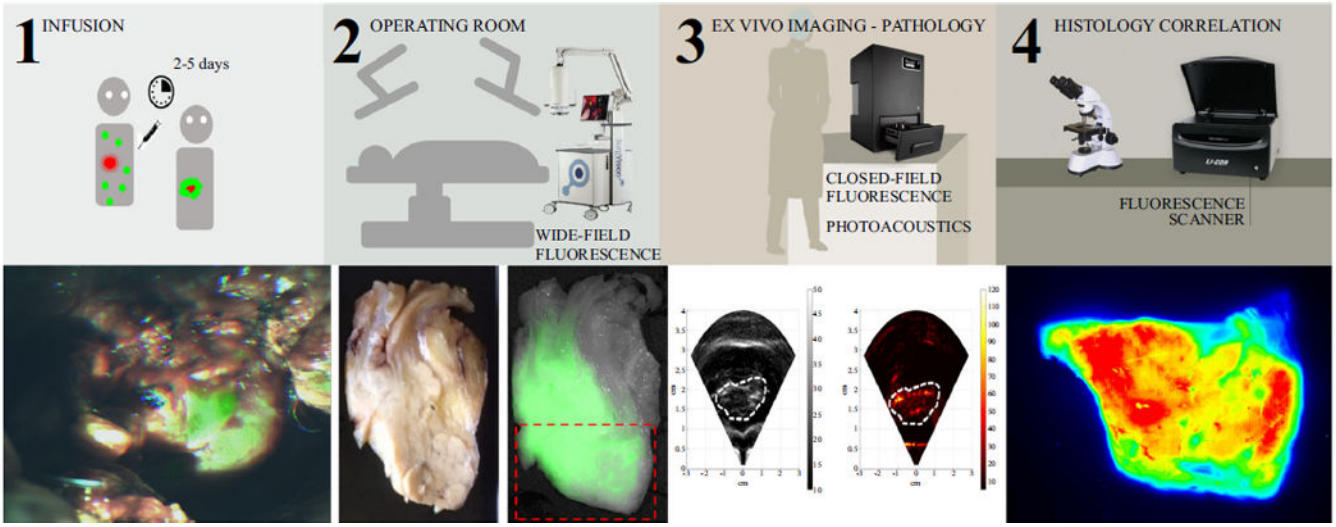

FIG. 1.

Workflow of clinical trial with imaging examples. **1. Infusion.** Infusion of a loading dose cetuximab (100 mg), and cetuximab-IRDye800 (50 or 100 mg) 2-5 days before surgical resection. **2. Operating room.** Intra-operative fluorescence imaging. **3. Ex vivo imaging—pathology.** *Ex vivo* fluorescenceand photoacoustic imaging of surgical specimens. **4. Histology correlation.** Histologic correlation between histologically proven tumor or normal tissue with H&E and fluorescent signal

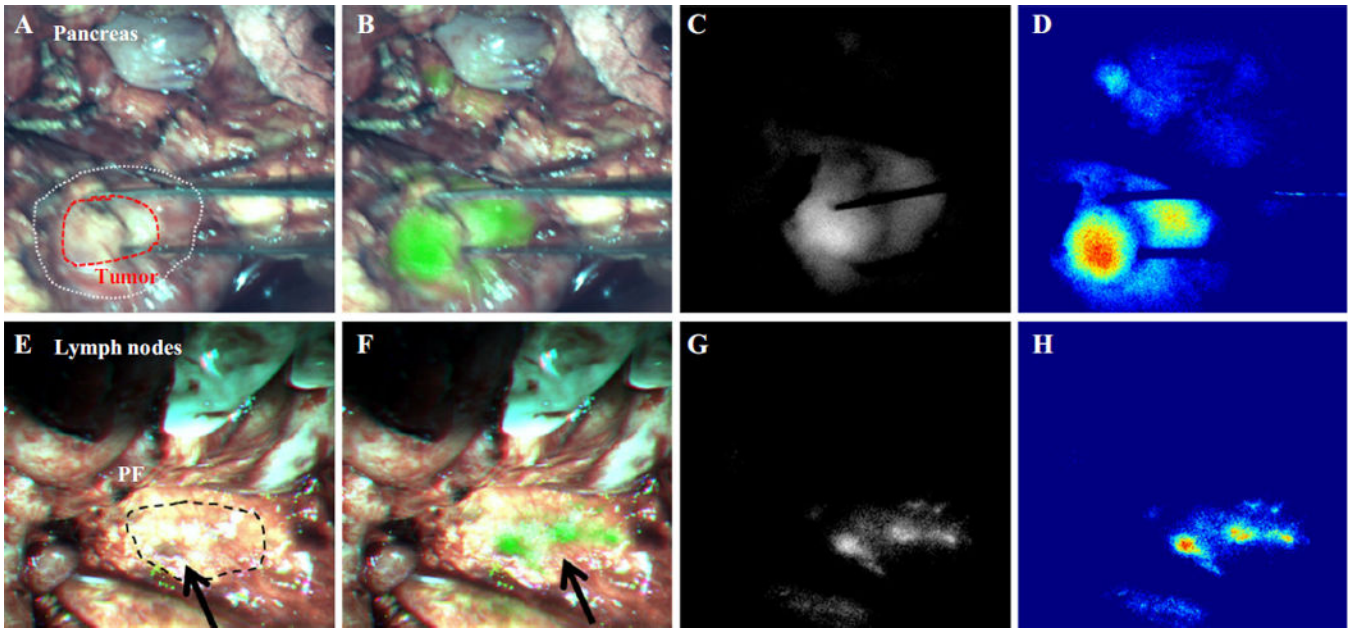

FIG. 2.

Intraoperative fluorescent imaging. Lesions could be clearly identified as shown in this figure; bright-field (**A** and **E**), overlay (**B** and **F**), grayscale (**C** and **G**), and heat-map (**D** and **H**) fluorescence imaging provided clear contrast between tumor and surrounding tissues during a Whipple procedure for both the primary tumor (**A–D**) and lymph nodes (**E–H**). *PF* peripancreatic fat

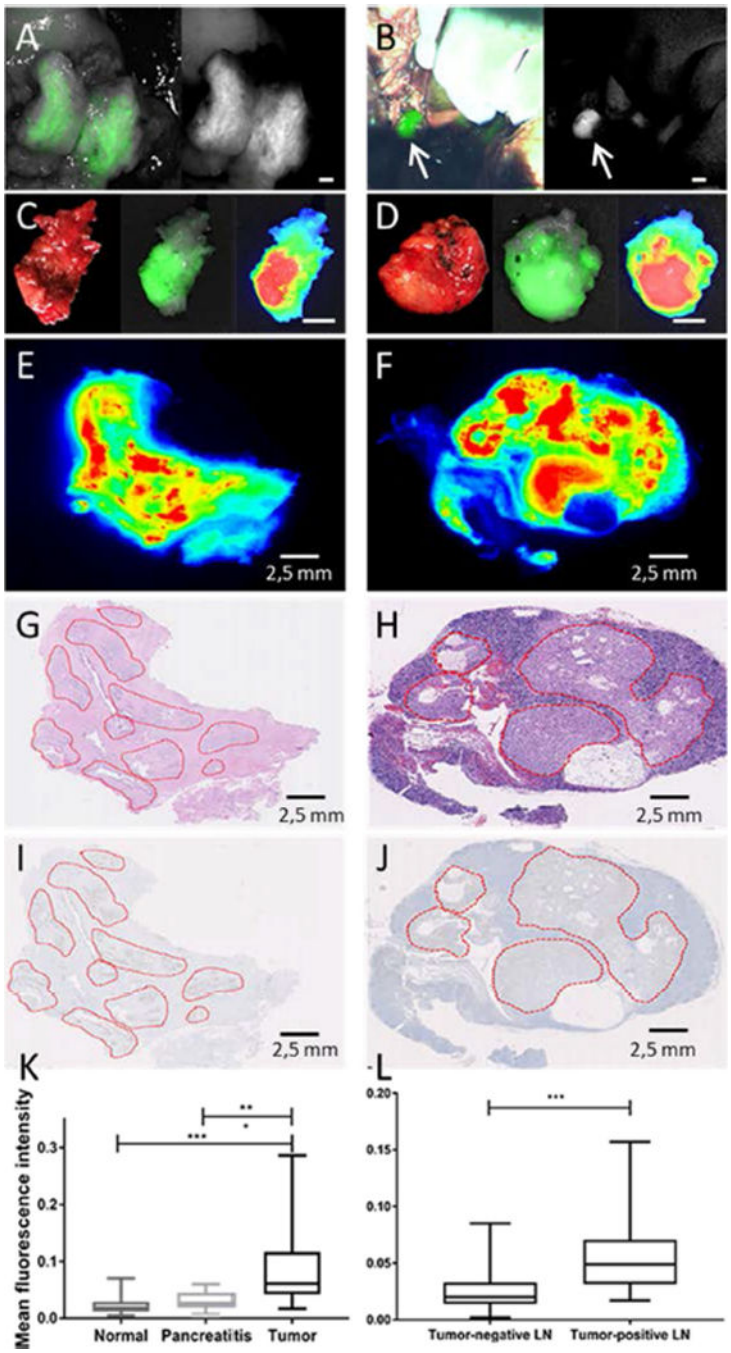

FIG. 3.

Correlation between intraoperative fluorescence and tumor-status. Identification of primary tumor (**A**) and tumor-bearing lymph node using fluorescence (**B**), with corresponding ex vivo fluorescence (**C** and **D**). Fluorescence of the primary tumor (**E**) is shown, and bisected lymph node on mesoscopic scale (**F**), with enhancements corresponding to the tumor on H&E, outlined in red (**G + H**)), and increased EGFR expression, also outlined (**I + J**). A graphic representation is shown of the mean fluorescence intensity (MFI) in normal

pancreatic tissue, pancreatitis and tumor (**K**), and tumor-bearing and tumor-negative nodes (**L**). Scale bar represents 1 cm, unless indicated differently. ***$p < 0.001$

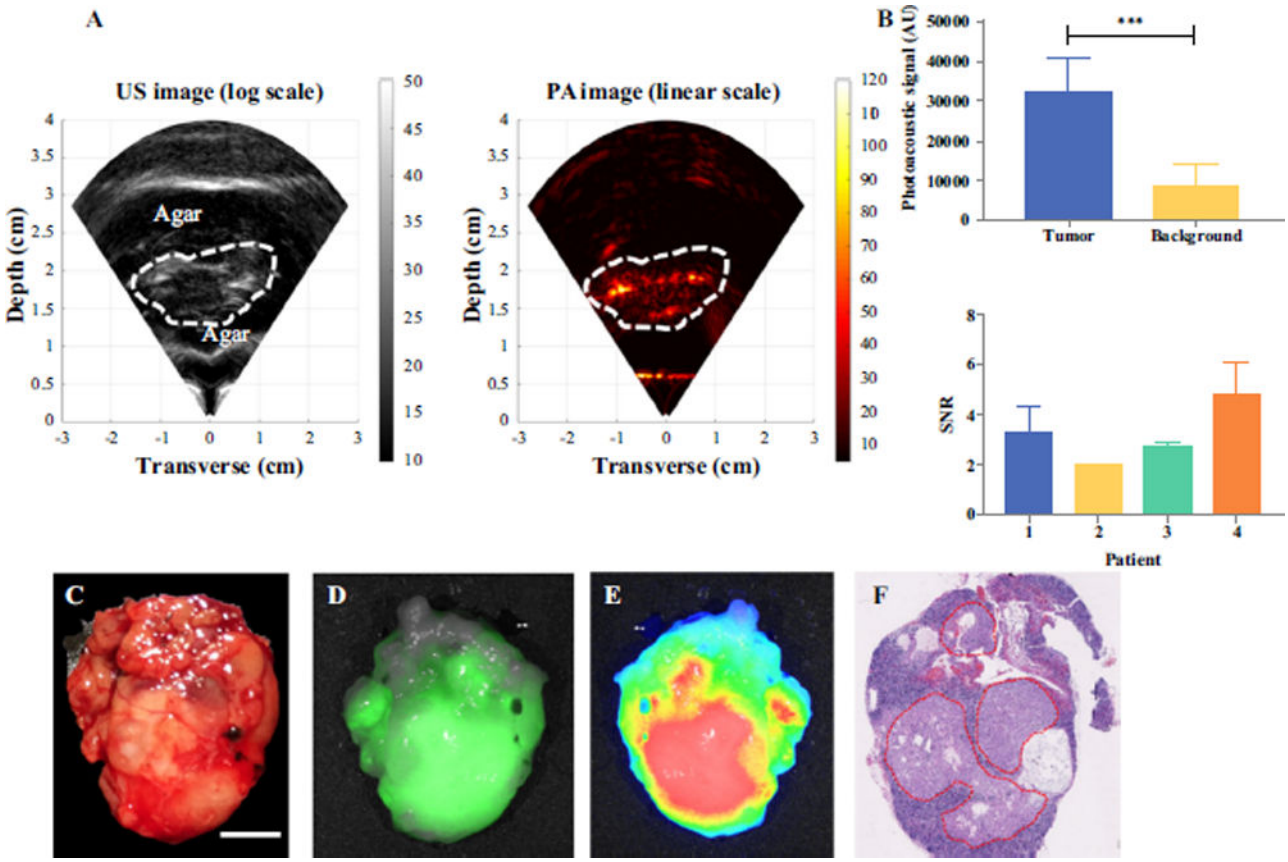

FIG. 4.

Photoacoustic and fluorescence imaging of tumor-bearing lymph node. Conventional ultrasound image of lymph node, surrounded by white dotted line and corresponding photoacoustic image (**A**). Mean photoacoustic signal in normal pancreatic tissue and tumor, and the signal-to-noise ratio (SNR) in photoacoustic signal per patient (**B**). Corresponding bright field (**C**), fluorescence overlay (**D**), heat-map fluorescent (**E**) images, and H&E section with outlined tumor (**F**) of tumor-bearing lymph node. ***$p < 0.001$. Scale bar represents 1 cm, unless indicated differently